Applied Catalysis B: Environmental 298 (2021) 120497

Contents lists available at ScienceDirect

Applied Catalysis B: Environmental

journal homepage: www.elsevier.com/locate/apcatb

Heterogeneous riboflavin-based photocatalyst for pollutant oxidation through electron transfer processes

Oscar Cabezuelo, Rebeca Martinez-Haya, Noelia Montes, Francisco Bosca *, M. Luisa Marin *

Instituto de Tecnología Química, Universitat Politècnica de València-Consejo Superior de Investigaciones Científicas, Avda. de los Naranjos s/n, Valencia, E-46022, Spain

ARTICLE INFO

Keywords:
Electron transfer process
Organic heterogeneous photocatalyst
Singlet excited state
Surface chemistry
Riboflavin

ABSTRACT

Organic photocatalysts could employ visible light to produce photodegradation of pollutants; however, their low photostability prevents their reuse even when they are supported on solid materials. Herein, to obtain a Riboflavin (RF)-based photocatalyst robust and recyclable, RF has been covalently anchored to silica particles, converting the known homogeneous photocatalyst into a new heterogeneous one (SiO_2-RF). To enhance the photostability of SiO_2-RF, generation of the RF triplet excited state and subsequent singlet oxygen were prevented by ensuring a complete shell of RF moieties on the silica spheres. Moreover, adsorption of organic pollutants such as phenol, *ortho*-phenylphenol, 2,4,6-trichlorophenol and pentachlorophenol on the surface of SiO_2-RF is favored in aqueous media, facilitating electron transfer from the pollutants to the short-lived first singlet excited state of RF. Photophysical measurements provided evidence on the photocatalytic mechanism for SiO_2-RF.

1. Introduction

The exponential growth of world population brings about with environmental problems due to the intensive exploitation of agriculture and the rapid industrial development required to face societal demands. The massive use of pesticides and fertilizers along with unrestricted industrial emissions are the main cause of surface water and groundwater contamination [1,2]. In this context, phenyl derivatives such as chlorophenols containing one or more chlorine atoms have extensively been used as pesticides and wood preservatives. They are additionally formed as by-products of water chlorination, combustion of organic matter, and even by incineration of municipal waste. They constitute a family of recalcitrant pollutants with a high biological risk due to its toxicity and poor biodegradation through the biological step in local wastewater treatment plants [3,4]. Moreover, they have been classified as toxic contaminants by the US Environmental Protection Agency (EPA) and the EC Environmental Directive (2455/2001/EC). Among them, 2-chlorophenol, 2,4-dichlorophenol, 2,4,6-trichlorophenol and pentachlorophenol have been included in the Priority Pollutants List of the EPA [5,6]. Other derivatives, like 2-phenylphenol are included in *the WHO Recommended Classification of Pesticides by Hazard* [7].

Advanced Oxidation Processes (AOPs) are based on the formation of highly reactive chemical species, which subsequently react with organic matter to produce more biodegradable molecules [8]. AOPs include a variety of treatments that have been applied for removing organic bio-recalcitrant pollutants and/or pathogens from wastewaters. Among the AOPs, photocatalysis, in which reactive species are created *via* light activation, constitutes an example of economical and green AOP, with high potential for wastewater remediation [9]. Photocatalytic processes can be homogeneous (*e.g.,* photo-Fenton, or mediated by excited species derived from organic photocatalysts), or heterogeneous (often based on the combination of solid semiconductors and light). The two main advantages of using organic photocatalysts in pollutants degradation are: i) their capacity to use visible light, and ii) the opportunity to elucidate the reaction mechanisms, based on the analysis of the kinetic behavior of the photogenerated transient species [10,11]. However, one of the major drawbacks of homogeneous organic photocatalysts is associated with their limited photostability, as they can suffer photobleaching or solvolytic attack in the reaction medium, thus its practical use is limited.

A representative example of organic photocatalysts is Riboflavin (RF), the water-soluble vitamin B, precursor of flavin mononucleotide and flavin dinucleotide in living-organisms [12]. RF can be found in water courses, where it could be responsible for the "naturally" occurring abatement of pollutants, including chlorophenols [10,13–23]. The chemical structure of RF is composed by a tricyclic system with a 7, 8-dimethyl substitution and a ribityl chain at the *N*-10 position. The

* Corresponding authors.
E-mail addresses: fbosca@itq.upv.es (F. Bosca), marmarin@qim.upv.es (M.L. Marin).

https://doi.org/10.1016/j.apcatb.2021.120497
Received 7 April 2021; Received in revised form 16 June 2021; Accepted 24 June 2021
Available online 29 June 2021

extended aromatic system in its tricyclic structure confers this photocatalyst the ability to absorb UV and visible light, showing two defined maxima at *ca.* 370 and 450 nm (see RF chemical structure in Scheme 1).

Redox potential of RF (E_{red} = -0.29 V *vs* NHE), combined with the energy of its excited states (E_S =2.48 eV and E_T =2.17 eV), turns RF into a moderate oxidant from its singlet and triplet excited states, with values of 2.19 V and 1.88 V, respectively [24–26].

Moreover, singlet oxygen ($^1O_2$), an important intermediate species in oxidation processes, is efficiently produced ($\Phi_\Delta = 0.49$) through energy transfer between ^{3}RF* and molecular oxygen (see Scheme 1) [12,24,26–28]. Kinetics studies carried out in RF-photocatalyzed degradation of several phenolic and chlorophenolic pollutants in homogeneous media, revealed efficient degradations. In these reactions, the participation of different species such as $^1O_2$, superoxide radical anion ($O_2^{\bullet-}$) and/or the singlet and triplet excited states of RF was envisaged [13,15,29–31].

However, RF displays low photostability associated with an intramolecular hydrogen rearrangement from the ^{3}RF* and also with the oxidation of the tricyclic system of RF by the generated singlet oxygen. As a consequence, reuse of RF is negligible, cutting down its suitability as a photocatalyst [32–34]. Thus, although ^{3}RF* is a key intermediate for most of the photocatalytic processes associated to RF, it is also responsible for its own photodegradation.

With this background, the aim of the present work is to design a recyclable and robust organic photocatalyst for wastewater remediation based on RF. Therefore, to achieve the first goal, RF will be incorporated into a heterogeneous support. In this sense, silica particles (SiO_2) will be used because they are cheap, easily available and offer high mechanical stability and well-known surface chemistry that would allow derivatization [35–37]. Moreover, to design a robust heterogeneous photocatalyst, a large number of RF molecules will be covalently anchored on the surface of the silica particles to prevent formation of ^{3}RF*. As a result, RF moieties will be close enough to produce, upon excitation, a quick deactivation from their singlet excited states, effect that has previously been described when agglomeration of RF molecules gives rise to the formation of RF dimers [38]. Thereafter, a fully photophysical characterization of this novel heterogeneous photocatalyst will be performed. Next, its photocatalytic potential and its photostability will be tested in the photodegradation of pollutants such as phenol (P), *ortho*-phenylphenol (OPP), 2,4,6-trichlorophenol (TCP) and pentachlorophenol (PCP), see Fig. 1. Moreover, a detailed kinetic study will help establish the mechanism of the observed photodegradations. Finally, a comparison between the performance of heterogeneous *vs* homogeneous RF will highlight the need for photophysical experiments in heterogeneous media, rather than assuming a similar mechanism to that in the homogeneous medium.

2. Experimental

2.1. Chemicals

Phenol (P), *orto*-phenylphenol (OPP), 2,4,6-trichlorophenol (TCP), pentachlorophenol (PCP), tetraethyl orthosilicate (TEOS), *p*-xylene, anhydrous triethylamine, perchloric acid, glacial acetic acid, acetic anhydride, dichloromethane, chloroform, magnesium sulfate and perinaphthenone were purchased from Sigma Aldrich. Anhydrous *N*,*N*-dimethylformamide and ammonium hydroxide (28–32 %) were purchased from Fischer. Riboflavin (RF), 3-(triethoxysilyl)propyl isocyanate (TPI), deuterated chloroform ($CDCl_3$) and deuterium oxide (D_2O) were purchased from TCI. Water used in the photodegradations was distilled grade, acetonitrile and ethanol of HPLC quality, dry toluene and acetone were purchased from Scharlab.

2.2. Instrumentation

All the instrumentation employed is described in Section 1 of SI.

2.3. Synthesis of SiO_2-RF

First, the synthesis of SiO_2 particles was carried out according to the Stöber method [39]. Thus, TEOS (1 mmol) was added to EtOH (500 mL) in the presence of NH_4OH (6.5 mmol) at 15 °C. After 2 h at this temperature, the reaction was conducted at room temperature for further 24 h. Afterwards, the obtained SiO_2 particles were centrifuged (4000 rpm for 5 min) and then washed with EtOH (3 × 150 mL). The resulting SiO_2 particles were dried under vacuum.

In parallel, the TPI_4RF intermediate was synthesized following a described procedure [35]. Briefly, a solution of RF (102 mg, 0.27 mmol), TPI (298 mg, 1.2 mmol) and Et_3N (250 μL, 1.8 mmol) in anhydrous DMF (50 mL) was heated at 70 °C for 48 h in a dry anaerobic atmosphere in the dark. Afterwards, the solvent was removed under vacuum and the crude product was submitted to the following step without any further purification.

Finally, a suspension of the above synthesized SiO_2 particles (1000 mg) with crude TPI_4RF (195 mg) and Et_3N (3 mL) in dry toluene (150 mL) was refluxed for 72 h, under N_2, in the dark. Afterwards, the functionalized particles were centrifuged (4000 rpm for 5 min) and then washed with acetone (3 × 10 mL). This crude was subsequently dried under vacuum to yield **SiO_2-RF** as a pale-yellow powder.

2.4. Quantification of the RF on the surface of SiO_2-RF

The percentage of RF on **SiO_2-RF** was made using two different methods: UV–vis absorbance and thermogravimetric analysis.

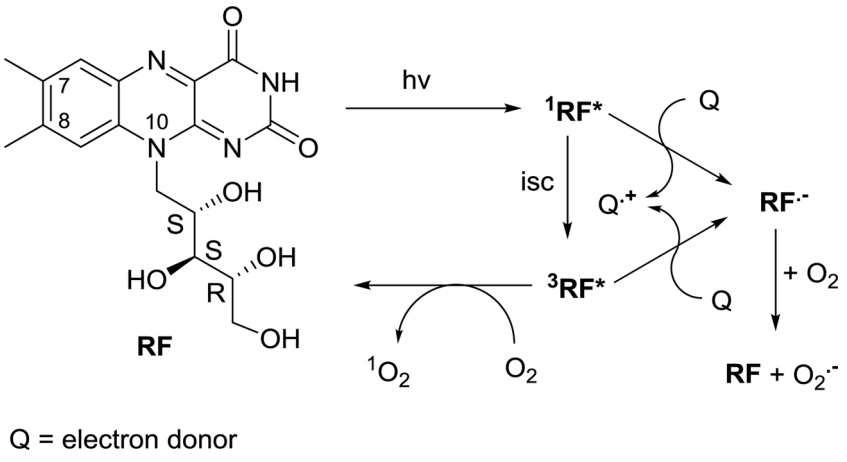

Scheme 1. Main reactive intermediates arising from Riboflavin (RF) photoexcitation.

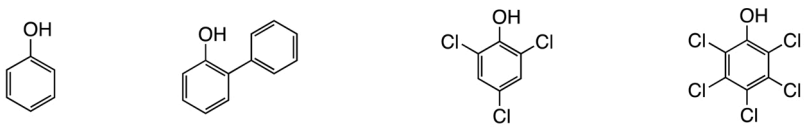

Phenol (**P**) | *orto*-Phenylphenol (**OPP**) | 2,4,6-Trichlorophenol (**TCP**) | Pentachlorophenol (**PCP**)

Fig. 1. Chemical structures of the selected phenolic pollutants.

2.4.1. Quantification of the RF on the surface of SiO_2-RF from UV–vis absorbance

The UV–vis absorbance of **SiO_2-RF** was compared to that obtained for riboflavin tetraacetate (RFTA, previously prepared according to a procedure already described in the literature [40], see Section 1 in the SI). For that purpose, the dispersion due to the heterogeneous **SiO_2-RF** (at 0.8 mg mL^{-1} in EtOH) was subtracted from its absorption spectrum applying the protocol detailed in Section 2 of SI. The resultant absorbance was 0.16 at 445 nm, which corresponds to a concentration of 1.37×10^{-5} M RF and consequently, the percentage of RF in the heterogeneous **SiO_2-RF** photocatalyst is 0.62 % (w/w).

2.4.2. Quantification of the RF on the surface of SiO_2-RF from thermogravimetric analysis

Thermogravimetric analysis (TGA) on SiO_2 and **SiO_2-RF** were also performed to quantify the percentage of RF. Hence, by comparing the observed loss in both materials, the estimated RF loading was 0.84 % (see more details in the SI Section 2 and Fig. S4).

2.5. Photophysical assays

2.5.1. Fluorescence measurements

Fluorescence quantum yields of **SiO_2-RF** and RFTA in EtOH:H_2O (4:1) were determined using RFTA in MeOH as reference [41]. Thus, the corresponding slopes of the linear fittings of the graphs emission *versus* absorbance for RFTA in EtOH:H_2O (4:1) and RFTA in MeOH, were compared to determine the fluorescence quantum yields of **SiO_2-RF** and RFTA in EtOH:H_2O (4:1). Details are provided in Section 3 of the SI.

Reactivity of singlet excited state of **SiO_2-RF** was determined using steady-state and time-resolved emission experiments. Hence, suspensions of **SiO_2-RF** (0.4 mg mL^{-1}, absorbance *ca.* 0.04 at $\lambda_{exc} = 375$ nm) in EtOH:H_2O (4:1), were treated with increasing concentrations of the phenolic contaminants, up to 90 mM. Parallel studies were performed using RFTA at the same absorbance.

When dynamic quenching is the only quenching mechanism, the Stern-Volmer equation, from steady-state experiments, is given by Eq. 1 [42]:

$$I^{\circ}/I = 1 + K_{SV}\,[Q] \quad (1)$$

if time-resolved experiments are performed, another expression for the Stern-Volmer equation is given by Eq. 2:

$$\tau^{\circ}/\tau = 1 + k_q\,\tau^{o}\,[Q] \quad (2)$$

In such case, the Stern-Volmer quenching constant (K_{SV}) from steady-state measurements is coincident to $k_q\,\tau^{o}$.

If quenching is also observed along with the decrease of the steady-state fluorescence (formation of a ground-state complex), an upward curvature would be observed for the plot I°/I *versus* [Q]; thus, a modified Stern-Volmer equation applies (Eq. 3):

$$I^{\circ}/I = (1 + K_{SV}\,[Q])\ x\ (1 + K_a\,[Q]) \quad (3)$$

Where K_a is the association constant for the formation of the "dark" complex. Rearrangement allows getting K_a from the linear fitting of $((I^{\circ}/I) - 1)/[Q]$ *versus* [Q], see Eq. 4:

$$((I^{\circ}/I) - 1)/[Q] = (k_q\,\tau^{o} + K_a) + k_q\,\tau^{o}\,K_a\,[Q] \quad (4)$$

In the case that quenching only occurs through the decrease of the steady-state emission ($k_q = K_{SV} = 0$), plot I°/I *versus* [Q] would give a linear plot; however, the slope corresponds to K_a. See how Eq. 3 simplifies to Eq. 5:

$$I^{\circ}/I = 1 + K_a\,[Q] \quad (5)$$

2.5.2. Laser flash photolysis experiments (LFP)

LFP measurements were performed using deaerated mixtures of **SiO_2-RF** (0.8 mg mL^{-1}, absorbance *ca.* 0.1 at $\lambda_{exc} = 355$ nm) in EtOH:H_2O (4:1). Control experiments were performed using a solution of RFTA in EtOH:H_2O (4:1) at the same absorbance with and without the silica particles.

Reactivity of triplet excited state of RFTA with pollutants was analyzed using deaerated solutions of RFTA (4×10^{-5} M, absorbance of 0.3 at $\lambda_{exc} = 355$ nm) in CH_3CN:H_2O (4:1), upon increasing concentrations of the phenolic pollutants (up 1 mM).

2.5.3. Singlet oxygen measurements

Two kinds of experiments were conducted:

On one hand, the ability of **SiO_2-RF** to form singlet oxygen ($^1O_2$) was tested. Thus, singlet oxygen generation from **SiO_2-RF** was measured under aerobic conditions using a suspension of 0.8 mg mL^{-1} in CH_3CN:D_2O (4:1). Control experiments were performed using a solution of RFTA in CH_3CN:D_2O (4:1) at the same absorbance with and without the silica particles.

On the other hand, reactivity of $^1O_2$, independently generated, with pollutants or RFTA was analyzed. Thus, aerated solutions of perinaphthenone (5.5×10^{-5} M) in CH_3CN:D_2O (4:1) were used as singlet oxygen generator due to its high singlet oxygen quantum yield. Then, lifetime of $^1O_2$ was recorded at 1270 nm upon increasing concentrations of the pollutants (up to 9×10^{-2} M) or RFTA (up to 2×10^{-4} M).

2.6. Adsorption of the pollutants on SiO_2-RF surface

The values were determined as follows: a suspension of **SiO_2-RF** (2.4 mg mL^{-1}) in the presence of P, OPP, TCP and PCP (5×10^{-5} M each) was stirred for 1 h in darkness. Then, two aliquots of 0.5 mL each were taken. The first one was filtered, diluted with 0.5 mL of EtOH and submitted to HPLC analysis (*vide infra*). The second aliquot was firstly mixed with 0.5 mL of EtOH and stirred for 10 min (to extract the adsorbed pollutants), then it was filtered and submitted to HPLC analysis. Thus, the adsorption values were determined from the difference of pollutants concentrations obtained between the two aliquots. Moreover, a solution of the four pollutants without the photocatalyst was used as a reference.

2.7. Photocatalytic degradation of the phenolic pollutants

Photochemical reactions were performed on a homemade

photoreactor built with 2.5 m strip blue-LEDs Samsung SMD5630 IP20 of 15 Wm^{-1}, spiral-shaped with the irradiation band centered at λ_{em} = 450 nm. The photoreactions were performed in test tubes with magnetic stirring under the specified atmosphere. To perform the photodegradations in the absence of oxygen, we proceed as follows: prior to irradiation N_2 was bubbled through the reaction mixture for 30 min. After that, the reaction tubes were sealed.

Aqueous mixtures (10 mL) containing one pollutant (2×10^{-4} M) or a mixture of the four pollutants (P, OPP, TCP and PCP, 5×10^{-5} M each, 2×10^{-4} M in total) and **SiO_2-RF** (2.4 mg mL^{-1}, 20 mol%) were stirred for 30 min in dark prior to irradiation, to reach the adsorption equilibrium between the pollutants and the photocatalyst. The progress of the photodegradations was monitored at different irradiation times by HPLC. For this purpose, 180 μL of a CH_3CN:H_2O (4:1) solution of *p*-xylene (3.2×10^{-4} M) as internal standard and 0.5 mL of EtOH were added to aliquots of 0.5 mL. The mixtures were stirred for 10 min to recover the adsorbed pollutants from the photocatalyst surface (see Section 2.6). Finally, each mixture was filtered with a CLARIFY-PTFE 13 mm syringe filter with 0.22 μm porous prior to HPLC analysis. All the experiments were performed in triplicates. A Mediterranean Sea 18 column (25cm × 0.46cm, 5 μm particle size) was employed for the HPLC studies. The mobile phase was fixed at 1.5 mL min^{-1} with an isocratic mixture of water at pH 3 (55 %) and acetonitrile (45 %). Aliquots of 90 μL were injected and the detection wavelength was fixed at 215 nm. With this sample treatment, monitoring by HPLC ensures detection of the real concentration of remaining phenol derivatives, adsorbed or in solution.

Photodegradations performed in acidic media (pH 3): For this purpose, a 10 mL solution of P, OPP, TCP and PCP (5×10^{-5} M each) was acidified with HCl 1 M until pH 3 prior to addition of **SiO_2-RF** (2.4 mg mL^{-1}). Then, the suspension was stirred for 30 min in darkness to allow adsorption to occur. After that, the reaction was conducted as described above for three consecutive runs. Before and after each consecutive run, the pH was monitored by a pH-meter to ensure that the pH of the suspension remain between 3.03 and 3.10.

Turnover numbers (TON) for the photocatalytic durability of the photocatalyst were calculated from the results of each consecutive run according to Eq. 6:

$$\mathrm{TON} = \frac{\text{moles of photodegraded pollutant}}{\text{moles of photocatalyst}} \quad (6)$$

Similar photoreactions were performed in homogenous aerated media. They were carried out under the same experimental conditions described for the heterogeneous ones but using acetylated riboflavin

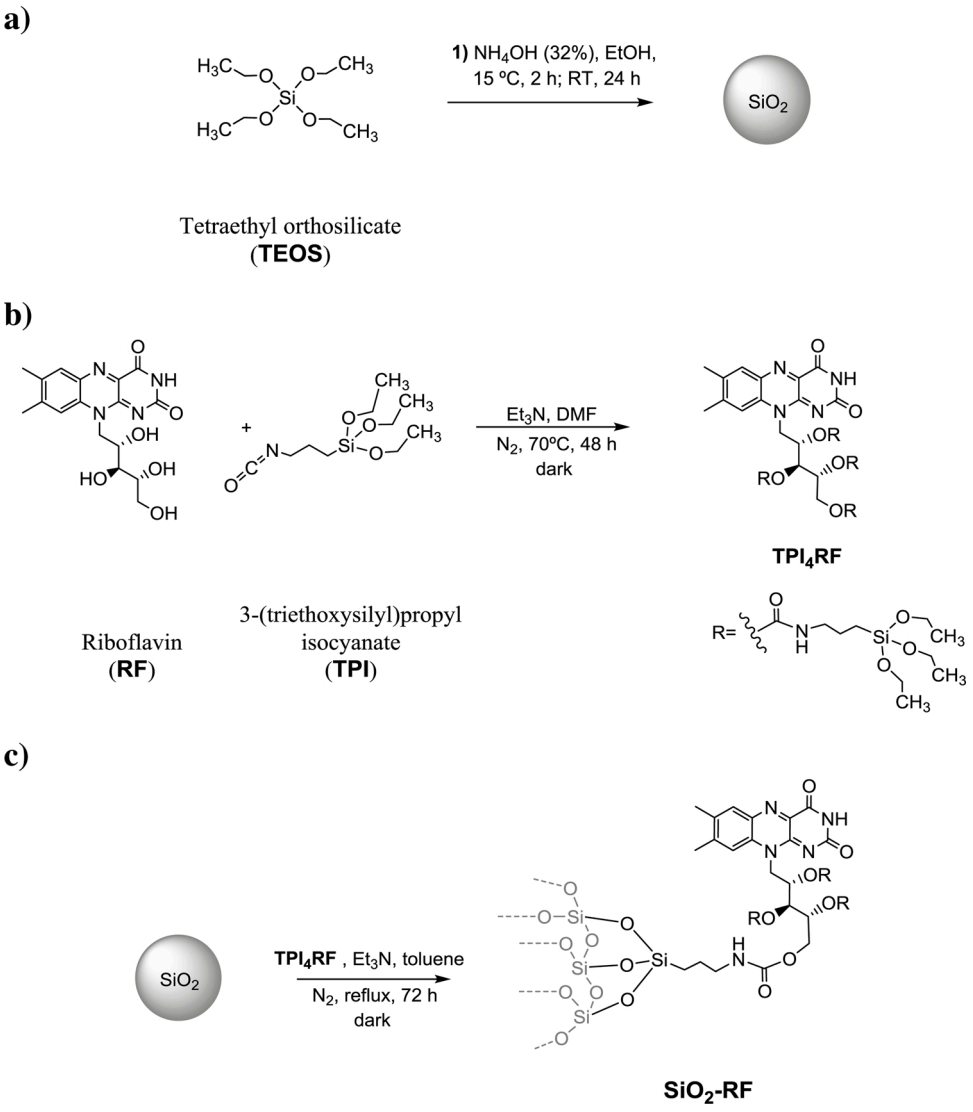

Scheme 2. Synthesis of the novel heterogeneous photocatalyst **SiO_2-RF** in three steps: a) SiO_2 particles preparation; b) RF derivatization; c) covalent linkage to get **SiO_2-RF**.

(RFTA, 4 × 10^{-5} M, 20 mol%) as photocatalyst. Degradation of the pollutants was also monitored by HPLC as described above.

2.8. Recyclability of SiO_2-RF

To evaluate the recyclability of **SiO_2-RF**, the mixture of the four pollutants and the **SiO_2-RF** was submitted to irradiation as described above and aliquots were taken up to 3 h. Then the reaction mixture was centrifuged (4000 rpm for 5 min); the supernatant was removed and the heterogeneous photocatalyst was washed with EtOH (3 × 20 mL). Finally, the photocatalyst was dried under vacuum for 2 h prior to the following use.

3. Results

3.1. Synthesis and characterization of the novel SiO_2-RF photocatalyst

The novel heterogeneous **SiO_2-RF** photocatalyst was synthesized as shown in Scheme 2. On one hand, SiO_2 particles were synthetized following the Stöber method [39], see Scheme 2a. In parallel, the ribityl side chain of the RF was derivatized by treatment with 3-(triethoxysilyl) propyl isocyanate (TPI) to get TPI_4RF, see Scheme 2b. The ^1H NMR of the crude was in agreement with the data previously described [35]. Finally, with the aim of synthesizing **SiO_2-RF** particles with their surfaces completely covered by RF, TPI_4RF was covalently attached to the surface of the SiO_2 particles upon treatment with Et_3N in dry refluxing toluene under anoxic atmosphere, for 72 h in dark, see Scheme 2c. The **SiO_2-RF** particles were obtained as a pale yellow powder.

Fig. 2 shows the TEM images corresponding to the SiO_2 particles (left column) and the **SiO_2-RF** photocatalyst (right column). The uncoated SiO_2 microparticles displayed spherical shape with a soft surface and an average diameter of 437 ± 8 nm (Fig. 2, left). Upon derivatization, the **SiO_2-RF** photocatalyst kept the spherical shape with a more roughness surface (right column) and a similar diameter (440 ± 15 nm, Fig. 2, bottom right).

The presence of RF on the photocatalyst was initially verified upon recording its diffuse reflectance spectrum. The absorbance (F(R)) was obtained by the Kubelka-Munk function (Fig. 3). The absorption spectrum of **SiO_2-RF** exhibits the characteristic bands of the RF chromophore (see Fig. S1): a strong band in the visible region peaking *ca.* 446 nm, and a less strong but still well-defined band in the UVA with a maximum at *ca.* 348 nm. The RF existence on the heterogeneous photocatalyst was also confirmed from the UV–vis spectrum of a suspension of **SiO_2-RF** in EtOH (Fig. S2). Moreover, a loading of 0.62 % RF (w/w) on the **SiO_2-RF** was estimated upon subtracting the dispersion obtained in this spectrum (see detailed procedure in the experimental Section 2.4.1. and Section 2 in SI). A slightly higher value (0.84 %) was obtained from TGA (see Section 2 in the SI).

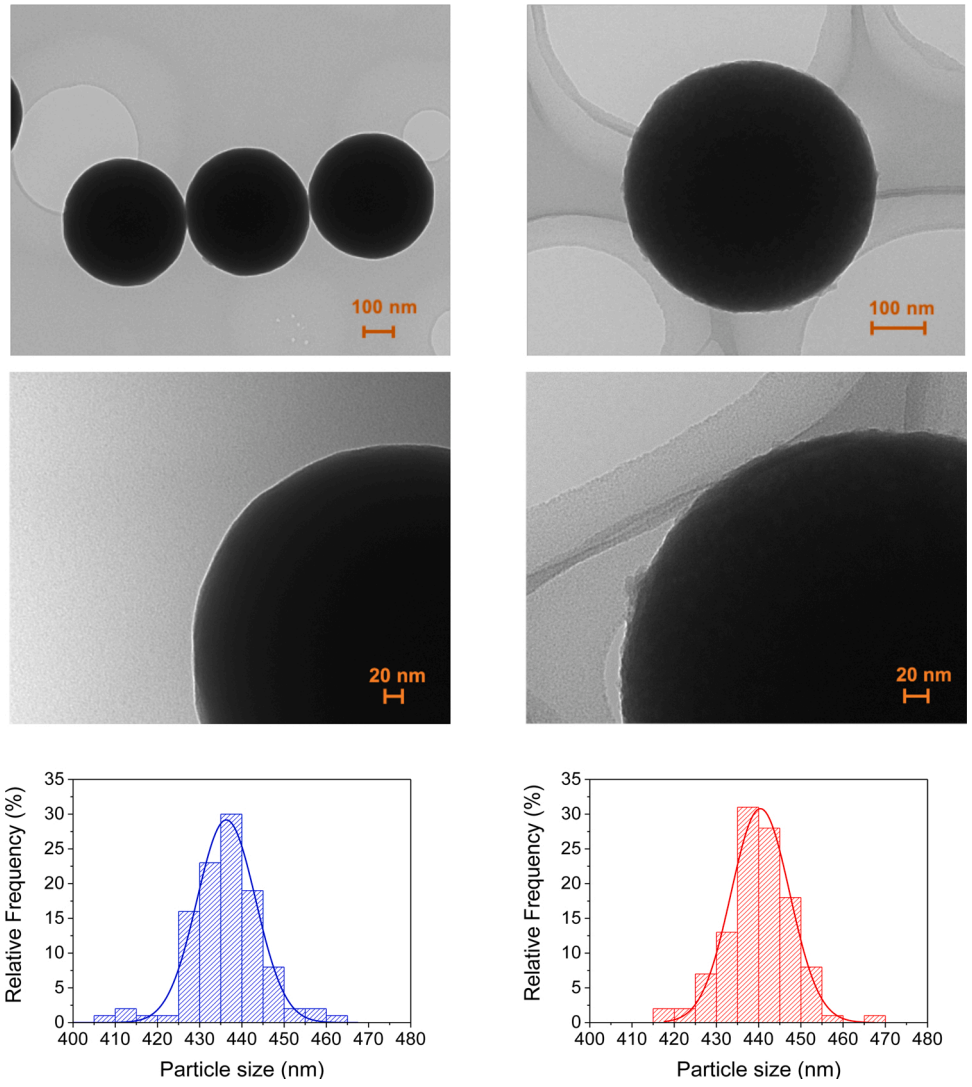

Fig. 2. TEM images and particle size distribution of the synthesized SiO_2 microparticles (left) and the **SiO_2-RF** photocatalyst (right).

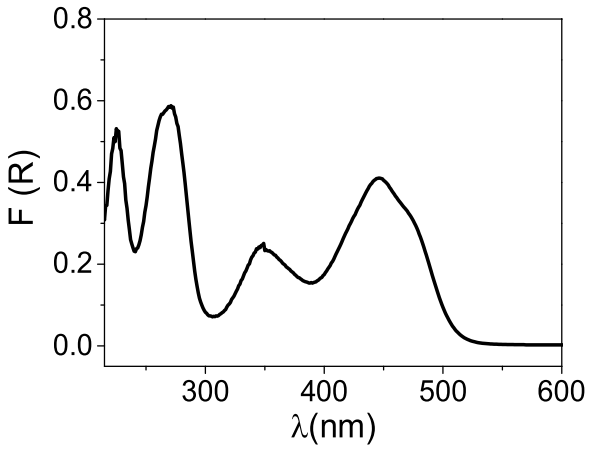

Fig. 3. UV–vis diffuse reflectance spectrum of the **SiO_2-RF** photocatalyst.

Additionally, with the aim at determining the proximity among the RF chromophores on the surface of the heterogeneous photocatalyst, we estimated the area occupied by the RF moieties covalently linked to the surface of **SiO_2-RF** (in $nm^2\ g^{-1}$) and compared this value to the total area of the particles. The detailed procedure followed to obtain both areas is described in Section 2 of the SI. Hence, a value of 5.80×10^{18} nm^2 of RF/g was calculated assuming the loading of 0.62 % RF (w/w) on the **SiO_2-RF**, while a total area of 5.14×10^{18} nm^2/g was determined for the **SiO_2-RF** particles. These area values ensure that the surface of the photocatalyst is completely covered by the RF moieties.

3.2. *Photophysical properties of SiO_2-RF*

Systematic photophysical experiments were carried out in order to evaluate if the formation of the triplet excited state of **SiO_2-RF** is prevented.

3.2.1. *The singlet excited state of SiO_2-RF*

Initially, the single excited state of the heterogeneous **SiO_2-RF** was characterized and compared to the homogenous RFTA. Surprisingly, when their steady-state emission spectra were compared under the same conditions, the emission intensity found for SiO_2-RF was lower than that obtained for RFTA in solution or in the presence of a suspension of SiO_2 (0.4 mg mL^{-1}, Fig. 4A). In fact, fluorescence quantum yield (Φ_F) determined for **SiO_2-RF** in EtOH:H_2O (4:1) was 0.02, while Φ_F for RFTA was 0.4 (see Section 3 of the SI). Besides, the emission maximum was red-shifted upon heterogeneization (531 nm *vs* 516 nm).

When time-resolved fluorescence experiments were performed in aerated EtOH:H_2O (4:1) media, the fluorescence lifetime (τ_F) determined for **SiO_2-^{1}RF*** was within the lamp pulse (Fig. 4B), which is much shorter than the value determined for RFTA in the same mixture of solvents ($\tau_F = 7.6$ ns) or those reported for the RF in aqueous media or acetonitrile (*ca.* 5 ns and 6.8 ns respectively) [43,44].

3.2.2. *The triplet excited state of SiO_2-RF*

Transient absorption spectrum of RFTA obtained from laser flash photolysis (LFP) displays a narrow band between 340 and 380 nm and a broad intense band from 500 to 700 nm, in agreement with the transient species reported in the literature for ^{3}RF* (see inset of Fig. 5) [25]. However, no signals were observed when the same experiment was performed using SiO_2-RF particles suspended in EtOH:H_2O (4:1). This result suggests that ^{3}RF* is either not generated or too short-lived to be recorded in a nanosecond time scale, when RF is linked to SiO_2 particles. Nonetheless, to discard the generation of ^{3}RF* with a very short lifetime due to the interaction of this transient species with the surface of SiO_2 particles, decay traces at 680 nm were monitored from RFTA solutions with and without the presence of SiO_2 particles (0.8 mg mL^{-1}) and using suspensions of **SiO_2-RF** (0.8 mg mL^{-1}). Results showed in Fig. 5 revealed that the absence of the triplet excited state in the case of **SiO_2-RF** in this

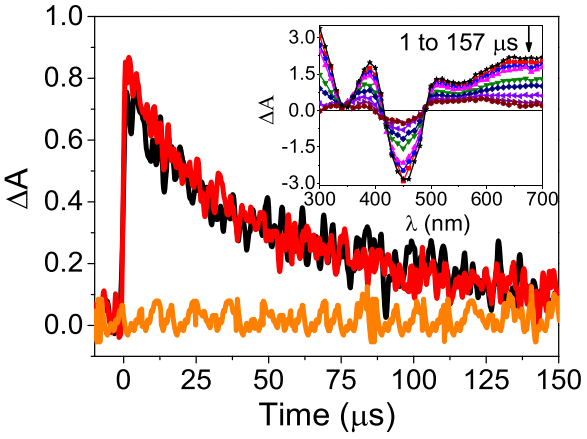

Fig. 5. Transient absorption decay traces recorded at 680 nm after laser pulse of a suspension of SiO_2-RF (orange), a solution of RFTA (black) and a solution of RFTA in a suspension (0.8 mg mL^{-1}) of the synthesized SiO_2 particles (red). All the experiments were carried out in deaerated EtOH:H_2O (4:1). Inset: Transient absorption spectra obtained upon LFP excitation of RFTA in deaerated ETOH:H_2O (4:1) (Abs = 0.3 at $\lambda_{exc} = 355$ nm). (For interpretation of the references to colour in this figure legend, the reader is referred to the web version of this article).

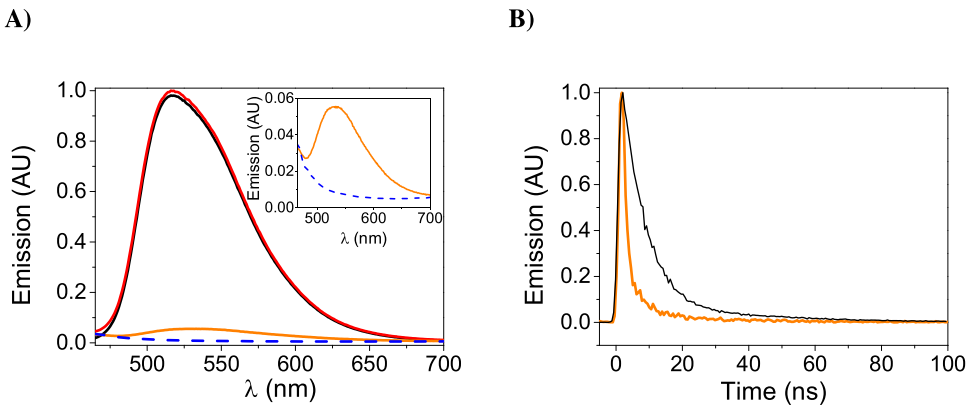

Fig. 4. Steady-state (A) and time resolved (B) emission of SiO_2-RF (orange), RFTA (black), RFTA in a suspension of the synthesized SiO_2 particles (red) and SiO_2 particles (0.4 mg mL^{-1}, dashed blue). Inset: zoom of the emission corresponding to SiO_2-RF and SiO_2, respectively. (Abs = 0.04 in EtOH:H_2O (4:1) at $\lambda_{exc} = 375$ nm). (For interpretation of the references to colour in this figure legend, the reader is referred to the web version of this article).

time scale is not connected to the presence of the SiO_2 particles. In fact, decay traces obtained from the RFTA solution do not show any change in absorption intensity or lifetime in the presence of SiO_2 particles.

3.2.3. Formation of $^1O_2$ from SiO_2-RF

In agreement with the results obtained for **SiO_2-RF** in LFP, the characteristic phosphorescence of $^1O_2$, which shows an emission maximum at 1270 nm, was not observed when a suspension of **SiO_2-RF** (0.8 mg mL^{-1}) was analyzed (Fig. 6). By contrast, a clear emission corresponding to $^1O_2$ was observed from RFTA solutions, even in the presence of a suspension of SiO_2 particles, see black and red traces, respectively in Fig. 6. In fact, singlet oxygen quantum yield (Φ_Δ) of RF in acetonitrile is reported to be 0.47 [28].

3.3. Adsorption of the pollutants on SiO_2-RF surface

The potential adsorption of the selected pollutants to the surface of the heterogeneous photocatalyst was tested. For this purpose, a suspension of **SiO_2-RF** (2.4 mg mL^{-1}) and P, OPP, TCP and PCP (5×10^{-5} M each) was stirred for 1 h in darkness to allow adsorption to occur, results are shown in Fig. 7. Thus, at the concentrations tested, OPP was completely removed from the solution, PCP showed *ca.* 80 % of adsorption of the initial concentration, while in the cases of P and TCP their affinity to the surface of **SiO_2-RF** was much lower (*ca.* 24 % and 22 % for P and TCP, respectively). These values revealed a relevant association between the heterogeneous photocatalyst **SiO_2-RF** and the pollutants which could be crucial to understand the mechanisms involved in the photodegradation of the contaminants.

3.4. Photocatalytic degradation of phenolic pollutants

The performance of the **SiO_2-RF** photocatalyst was evaluated in the removal of the selected phenolic pollutants in aqueous aerobic media under visible LED light irradiation.

A mixture of each pollutant independently (P, OPP, TCP or PCP, 2×10^{-4} M each) or all the pollutants together (P, OPP, TCP and PCP, 5×10^{-5} M each) and **SiO_2-RF** (2.4 mg mL^{-1}, 20 mol%) were irradiated under LED light centered at 450 nm, see Fig. 8. Selected pollutants were removed within 12 h. Even more, in the first 4 h, the removal percentages were as high as: 83 %, 88 %, 98 % and 97.5 % for P, OPP, TCP and PCP respectively, when they were irradiated separately (Fig. 8A), and slightly higher (84 %, 100 %, 99 % and 98 % for P, OPP, TCP and PCP, respectively), when they were irradiated together (Fig. 8B). Values

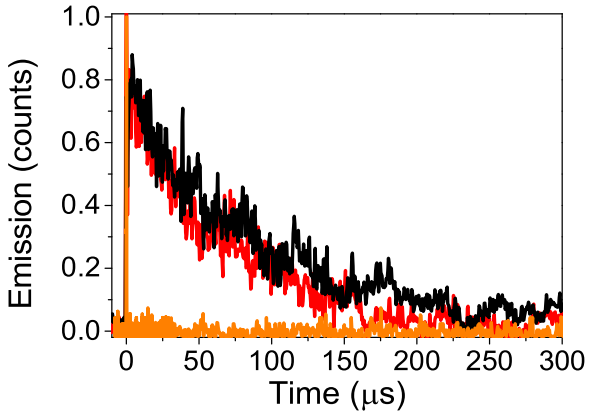

Fig. 6. Emission decays recorded at 1270 nm after laser pulse of a suspension of SiO_2-RF (orange), a solution of RFTA (black) and a solution of RFTA in a suspension of the synthesized SiO_2 particles (red). All the experiments were carried out in aerated CH_3CN:D_2O (4:1) (Abs = 0.1 at λ_{exc} = 355 nm in all cases). (For interpretation of the references to colour in this figure legend, the reader is referred to the web version of this article).

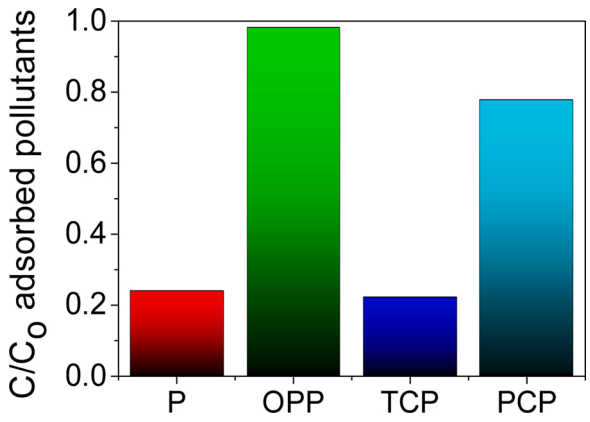

Fig. 7. Fraction of the four phenolic pollutants ($C_o = 5 \times 10^{-5}$ M each one) adsorbed on the surface of **SiO_2-RF** photocatalyst (2.4 mg mL^{-1}).

shown in the graphs of Fig. 8 are the averages of three independent runs.

Irradiation of the mixture of contaminants was also performed in the absence of oxygen (see Fig. 9). Although the abatement of the pollutants was eventually completed upon 12 h irradiation, the smaller percentages of removal achieved in the first 4 h (62 %, 94.5 %, 26 % and 21 % for P, OPP, TCP and PCP, respectively) is in agreement with the involvement of O_2. Furthermore, a plausible explanation for the different photodegradation of the phenol derivatives in the absence of O_2 could be found on the basis of the oxidation potentials of the phenol derivatives [45]. Hence, upon reaction with the singlet excited state of RF, the generated radical cations, in the absence of O_2, would take an electron from the derivatives with lower oxidation potential, eventually giving rise to the formation of dimers.

Control experiments showed no photodegradation at all in the absence of light (Fig. S13 in SI). Furthermore, in an attempt to investigate the advantages of **SiO_2-RF** *versus* RF, similar studies were carried out in aqueous media using RFTA, as a more stable RF derivative in homogeneous media [43]. The results of the homogeneous photodegradations, performed under the same experimental conditions (each pollutant separately or all together), are shown in Fig. 10.

Homogeneous photodegradations exhibited faster degradation rates than the heterogeneous ones during the first hour (see Figs. 8 and 10); however, even after 12 h irradiation, the pollutants did not reach 100 % abatement, except in the case of OPP when the pollutants were irradiated separately (Fig. 10A), and PCP when they were irradiated simultaneously (Fig. 10B). Even using the more stable RFTA as homogeneous photocatalyst [43], decoloration of the irradiation mixtures was observed in few hours. Thus, in agreement with degradation of the homogeneous photocatalyst, the abatement of the pollutants seems to stop before the third hour, contrarily to the **SiO_2-RF**. A further advantage of the heterogeneous **SiO_2-RF** relies on their potential reusability. For this purpose, the efficiency of the novel photocatalyst was evaluated up to three runs (Fig. 11). The phodegradation of the pollutants mixture was stopped after 3 h irradiation. Upon, centrifugation, filtration, washing and drying, the photocatalyst was employed in two further consecutive runs, keeping in the third one up to the 62 % of its original activity. In other words, the calculated TON upon 3 h photodegradation decreased from 4.5 to 3.1 and 2.8 in three consecutive runs. Deactivation of the photocatalyst due to a partial degradation of the RF linked to the SiO_2 surface could not be discarded due to the organic nature of the RF molecule.

The heterogeneous photocatalytic degradation using **SiO_2-RF** photocatalyst was also evaluated under acidic media. The adsorption of the phenol derivatives on the **SiO_2-RF** surface was clearly pH dependent (see Fig. S14). In fact, P, OPP and TCP showed negligible affinity for the photocatalyst surface, while the affinity of PCP was lower than the one observed at neutral pH 60 % *vs* 80 %). Under this scenario the efficiency

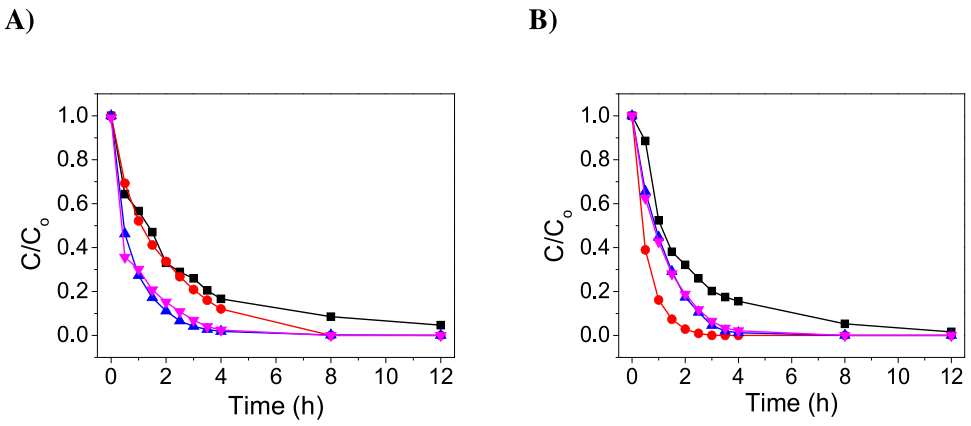

Fig. 8. Heterogeneous photocatalytic degradation of P (■), OPP (●), TCP (▲) and PCP (▼) irradiated separately ($C_o = 2 \times 10^{-4}$ M each, A) and simultaneously ($C_o = 5 \times 10^{-5}$ M each, B) with LED light centered at 450 nm in aerated aqueous solutions, in the presence of **SiO_2-RF** (2.4 mg mL^{-1}).

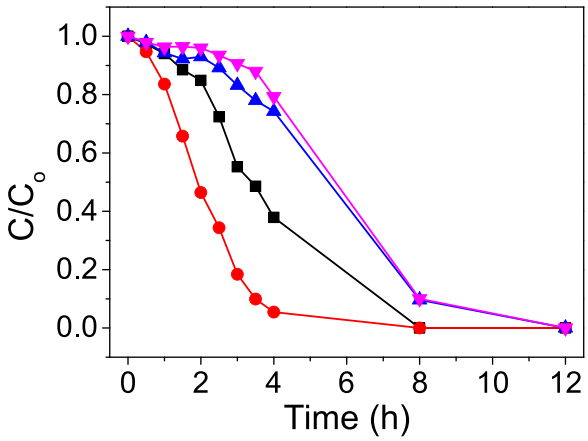

Fig. 9. Heterogeneous photocatalytic degradation of P (■), OPP (●), TCP (▲) and PCP (▼) ($C_o = 5 \times 10^{-5}$ M each) irradiated with light centered at 450 nm simultaneously in deaerated aqueous solutions, in the presence of **SiO_2-RF** (2.4 mg mL^{-1}).

of the photocatalytic degradations at pH 3 was clearly lower than at neutral pH (see Fig. S15).

3.5. *Involvement of the excited states of SiO_2-RF/RFTA and participation of singlet oxygen*

First, the interaction between the singlet excited state of **SiO_2-^{1}RF*** and the contaminants was examined on the basis of steady-state and time-resolved emission experiments. Thus, aerated suspensions of the photocatalyst in EtOH:H_2O (4:1) were excited at 375 nm in the absence and in the presence of increasing concentrations of the pollutants (Fig. 12). Hence, efficient steady-state quenching emissions were obtained for each pollutant (the corresponding I°/I *versus* [Q] plots are shown in the inset of each graph and the obtained constants are in Table 1). However, time-resolved experiments performed with **SiO_2-RF** did not show any fluorescence lifetime change upon increasing concentrations of the pollutants, which indicates that the dynamic contribution to the quenching process is negligible. Consequently, formation of ground state complexes between the **SiO_2-RF** and the pollutants is inferred, and the determined association constants (K_a) from steady-state measurements, indicated that they are particularly favored in the case of PCP.

By contrast, results from the steady-state and time-resolved experiments performed using RFTA in homogeneous media (Fig. S8 in SI) showed an upward curvature in the I°/I *versus* [Q], revealing the existence of dynamic and static fluorescence quenching processes (see experimental section). From the time-resolved experiments, the rate constants for the quenching of ^{1}RFTA* by the pollutants were diffusion

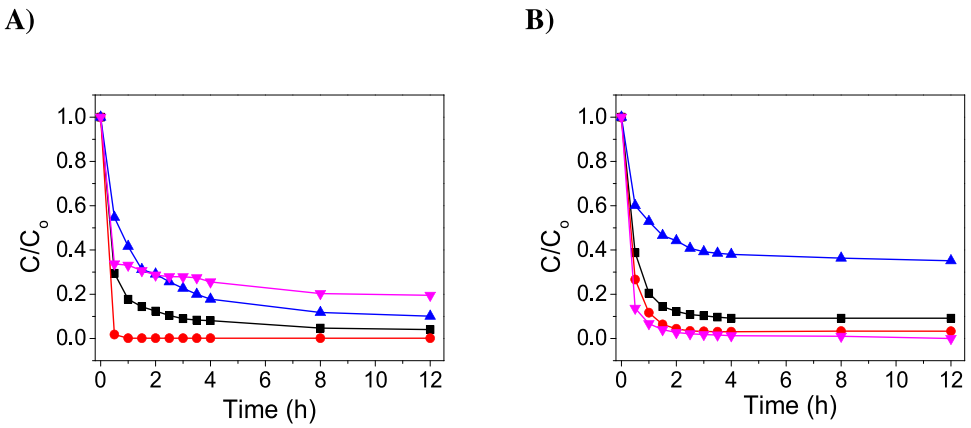

Fig. 10. Homogeneous photocatalytic degradation of P (■), OPP (●), TCP (▲) and PCP (▼) irradiated separately ($C_o = 2 \times 10^{-4}$ M each, A) and simultaneously ($C_o = 5 \times 10^{-5}$ M each, B) with LED light centered at 450 nm in aerated aqueous solutions, in the presence of RFTA (4×10^{-5} M).

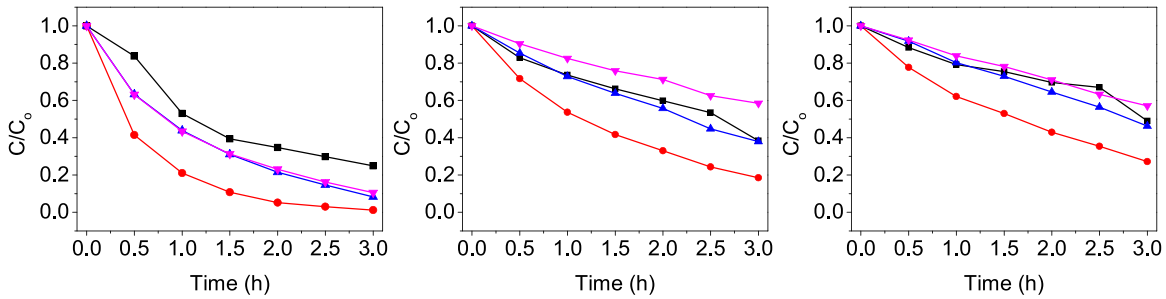

Fig. 11. Heterogeneous photocatalytic degradation of P (■), OPP (●), TCP (▲) and PCP (▼) ($C_o = 5 \times 10^{-5}$ M each) irradiated simultaneously with light centered at 450 nm in aerated aqueous solutions in the presence of **SiO_2-RF** (2.4 mg mL^{-1}) for 3 h for three consecutive runs.

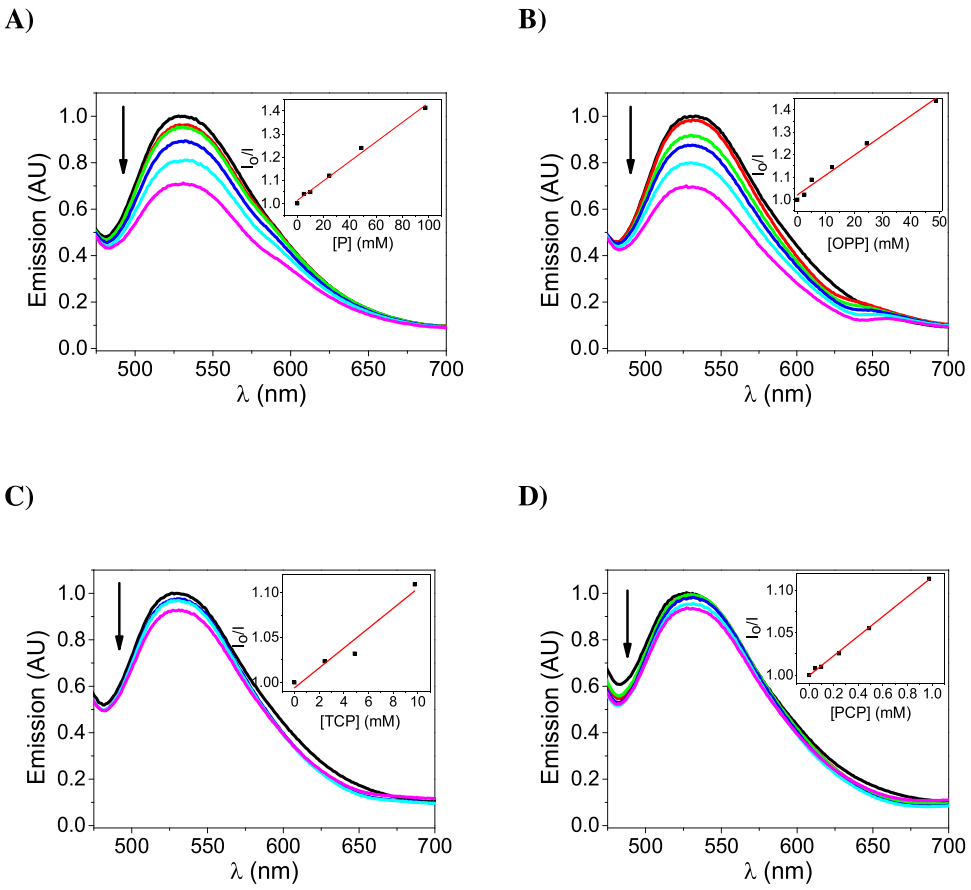

Fig. 12. Steady-state emission quenching of **SiO_2-RF** in an aerated EtOH:H_2O (4:1) suspension upon addition of increasing concentrations of P (A), OPP (B), TCP (C) and PCP (D) (Abs = 0.04 at λ_{exc} = 375 nm). Insets: Corresponding Stern-Volmer plots.

Table 1
Constants values determined for the quenching of the emission of **SiO_2-^{1}RF*** and **^{1}RFTA*** by the phenolic pollutants in aerated EtOH:H_2O (4:1).

Contaminant	SiO_2-^{1}RF*	^{1}RFTA*	
	Steady-state K_a (M^{-1})	Steady-state K_a (M^{-1})	Time-resolved k_q x 10^{-9} ($M^{-1}s^{-1}$)
P	4.2	6.3	4.3
OPP	8.8	12.2	4.8
TCP	11.0	9.1	3.7
PCP	116.2	138.0	–

controlled in all cases, except from PCP (Table 1) [46]. Moreover, plot of ((I°/I) - 1) / [Q] *versus* [Q] allowed determining the association constants in homogeneous media (Table 1). The obtained results in the case of PCP would be due to its low solubility in the experimental conditions.

Participation of the ^{3}RFTA* in the homogeneous photodegradations was investigated by LFP. The determined quenching rate constants for the different pollutants are quite similar (see Table 2). Kinetic traces of the experiments and the Stern-Volmer fittings are show in Fig. S9. Moreover, the formation of the corresponding reduced species of RFTA

Table 2
Rate constants for quenching of ^{3}RFTA* or $^1O_2$ by P, OPP, TCP and PCP in CH_3CN:H_2O (4:1) or CH_3CN:D_2O (4:1), respectively.

Contaminant	^3k_q x 10^{-9} ($M^{-1}s^{-1}$)	$k_{q,1O2}$ x 10^{-5} ($M^{-1}s^{-1}$)
P	0.57	1.6
OPP	1.31	3.4
TCP	0.93	2700
PCP	1.41	2700

($RFTA^{\bullet-}$) was detected from these LFP experiments through its characteristic transient absorption spectrum (see Figure S10 in SI) [10,47].

Finally, reactivity of $^1O_2$ with the pollutants, as well as with RFTA, was evaluated. Interestingly, the quenching rate constants for TCP and PCP were higher than those obtained for P and OPP (see values in Table 2 and the kinetic traces and the corresponding Stern-Volmer fitting in Figs. S11 and S12 of the SI). Besides, a $^1O_2$ quenching rate constant of 1.1×10^7 M^{-1} s^{-1} was determined for RFTA, which is similar to that described in the literature [48].

4. Discussion

TEM images of the synthesized **SiO_2-RF** showed a homogeneous surface (see Fig. 2); the diameter of the particles, before and after the covalent junction, exhibited a Gaussian distribution, with the expected increase upon derivatization. **SiO_2-RF** exhibited the characteristic UV–vis spectrum of the RF chromophore as shown in Fig. 3. Loading studies revealed that the percentage of RF (w/w) on the **SiO_2-RF** may be between the 0.62 %, determined using a comparative method of the UV–vis spectra of the RFTA and **SiO_2-RF**, and the 0.84 % estimated by comparing the TGA of SiO_2 particles with that obtained for **SiO_2-RF** (see details in Section 2.4 and in the SI). Interestingly, even the minimum loading value determined (0.62 %, w/w), guarantees a complete cover of the surface of the SiO_2 particles according to our estimations (see details in the Section 2 of the SI).

To analyze the expected changes in the photophysical properties of RF when linked to the surface of **SiO_2-RF**, photophysical experiments were performed with suspensions of the heterogeneous **SiO_2-RF** and compared to those carried out with solutions of RFTA. Hence, steady-state and time-resolved fluorescence studies performed with **SiO_2-RF** and RFTA revealed great differences in the emission properties (see Fig. 4). In fact, the fluorescence quantum yield of **SiO_2-^{1}RF*** ($\Phi_F = 0.02$) and its lifetime (within the lamp pulse) were clearly smaller than those of ^{1}RFTA* ($\Phi_F = 0.4$ and $\tau^o = 7.6$ ns, similar to the reported ones for RF) [43]. As expected, these differences indicated that a new and very efficient fluorescence deactivation pathway appeared upon linking the chromophore to the surface of the SiO_2 particles. Moreover, the emission maximum was red-shifted upon heterogeneization (531 nm *vs* 516 nm) indicating an increase of the electronic delocalization for the first singlet excited state of **SiO_2-^{1}RF***. These results acted as an unambiguous evidence of the expected pi-pi stacking interactions between chromophore dimers. Thus, the most likely deactivation pathway of the first singlet excited state of the heterogeneous photocatalyst (**SiO_2-^{1}RF***) seems a charge transfer interaction with close ground state RF moieties. Next, formation of the triplet excited state was investigated by means of the laser flash photolysis technique. In this case, no signal was observed from **SiO_2-RF**, indicating that the deactivation of the singlet excited state follows an efficient pathway that prevents intersystem crossing to the triplet excited state (Fig. 5). Accordingly, $^1O_2$ was not generated (Fig. 6). The achieved photophysical properties of **SiO_2-RF** indicated that its photostability should have been improved in comparison with RF or RFTA.

Nevertheless, to work as a photocatalyst from its short-lived **SiO_2-^{1}RF***, it is crucial to exhibit a high adsorption capability. This property was evaluated from aqueous mixtures of the four pollutants (P, OPP, TCP and PCP, 5×10^{-5} M each) and **SiO_2-RF** (2.4 mg mL^{-1}, 20 mol %). Results shown in Fig. 7 revealed that *ca.* 56 mol% of the pollutants were adsorbed on the surface of the photocatalyst. This result validated the excellent adsorption capability of the new photocatalyst and ensured a high proximity between RF chromophore and the pollutants. In fact, at the employed photocatalyst concentration (2.4 mg mL^{-1}, 20 mol%) a ratio RF:pollutants is *ca.* 1:3 on the surface of **SiO_2-RF**. Moreover, it could be anticipated that other contaminants, in general with higher molecular size, will show at least similar adsorption affinity.

The photocatalytic performance of **SiO_2-RF** in the removal of the selected phenolic pollutants, see Fig. 8, revealed complete abatement of the contaminants within the first 4 h, regardless the photodegradations took place with a mixture of all the pollutants or with each individual one. It should be noted that, when photodegradation was performed with the mixture of the four pollutants, there is a clear correlation between the pollutants' photodegradation half-lives and the percentage of pollutant adsorbed to the surface (see Figs. 7 and 8B). This fact clearly confirmed that photodegradation mediated by **SiO_2-RF** is always produced on the adsorbed pollutants. The different degradation half-lives showed by the pollutants when they were irradiated independently in the presence of **SiO_2-RF**, could be attributed to different efficiencies of back electron transfer processes.

By contrast, when the photocatalyzed degradation was performed in the presence of homogeneous RFTA, fast pollutants' degradation was observed in the first 30 min; however, the photocatalytic activity stopped after the first one-two hours without achieving complete photodegradation (Fig. 10).

Systematic photophysical experiments were carried out in order to establish the mechanism operating in the heterogeneous/homogeneous photocatalyzed degradation of the phenolic pollutants. Specifically, the involvement of the excited states of **SiO_2-RF**/RFTA and the formation of singlet oxygen was investigated.

Thus, static and dynamic fluorescence quenching of **SiO_2-^{1}RF*** and ^{1}RFTA* by the pollutants was evaluated to determine the reactivity of both singlet excited states (see Table 1). The steady-state studies revealed that static quenching is operating in homogeneous and heterogeneous media (Table 1). However, when the lifetime of **SiO_2-^{1}RF*** was analyzed in the presence of the pollutants, no changes were detected, probably due to its very low lifetime, thus a dynamic interaction between the pollutants and **SiO_2-^{1}RF*** must be a minor process. By contrast, high values, close to the diffusion limit, were found for the dynamic quenching of ^{1}RFTA* by P, OPP and TCP but not by PCP. The result of the homogeneous experiments were not unexpected, since thermodynamic calculations anticipated exergonic electron transfer from phenol derivatives (with oxidation potentials between 0.7 and 0.9 V) to ^{1}RFTA* (redox potential of RF *ca.* -0.29 V and E_S *ca.* 2.48 eV) [24,25,45,49].

Furthermore, since **SiO_2-^{3}RF*** is not formed, the photodegradation of the pollutants by **SiO_2-RF** cannot be attributed to the triplet excited state nor to $^1O_2$. On the contrary, ^{3}RFTA* was detected (see Fig. 5) and it is efficiently quenched by all the pollutants with kinetic quenching constants close to the diffusion limit (Fig. S9 and Table 2) [46]. Besides, the corresponding transient spectra obtained from mixtures of RFTA and the pollutants revealed the formation of the corresponding reduced species ($RFTA^{\bullet-}$) (see Fig. S10) [10]. Moreover, generation of $^1O_2$ from RFTA was confirmed thought time-resolved emission studies (Fig. 6) and its quenching by the pollutants revealed higher reactivity for chlorophenols than for P and OPP (see Fig. S11 and Table 2). It is worth to mention that the reactivity of $^1O_2$ with RFTA is higher (1.1×10^7 $M^{-1}s^{-1}$, Fig. S12) than that of P or OPP which means that, in homogeneous media, this reactive oxygen species would produce a faster oxidation of RFTA than that of P or OPP.

All these photophysical results clearly demonstrate that the operating mechanism in the photocatalytic behavior of **SiO_2-RF** cannot be predicted from the behavior of the homogeneous RFTA.

The photodegradation tests agreed with the different behavior observed for RF chromophore in the photophysical studies of RFTA and **SiO_2-RF**. More specifically, a kinetic analysis of the data obtained in the photophysical studies of RFTA taking into account the initial concentration of the pollutants (2×10^{-4} M) and the molecular oxygen in aqueous media (2.7×10^{-4} M) indicates that an electron transfer reaction between ^{3}RFTA* and the pollutant Q to generate $RFTA^{\bullet-}$ and $Q^{\bullet+}$ would be the main photodegradation pathway during the first minutes (Scheme 3). A similar analysis has been clearly explained in a precious study using RF with phenol [15]. Thus, the slow photodegradation observed using **SiO_2-RF**, where similar radicals (**SiO_2-RF$^{\bullet}$**− and $Q^{\bullet+}$) are generated, would be attributed to a higher back electron transfer process

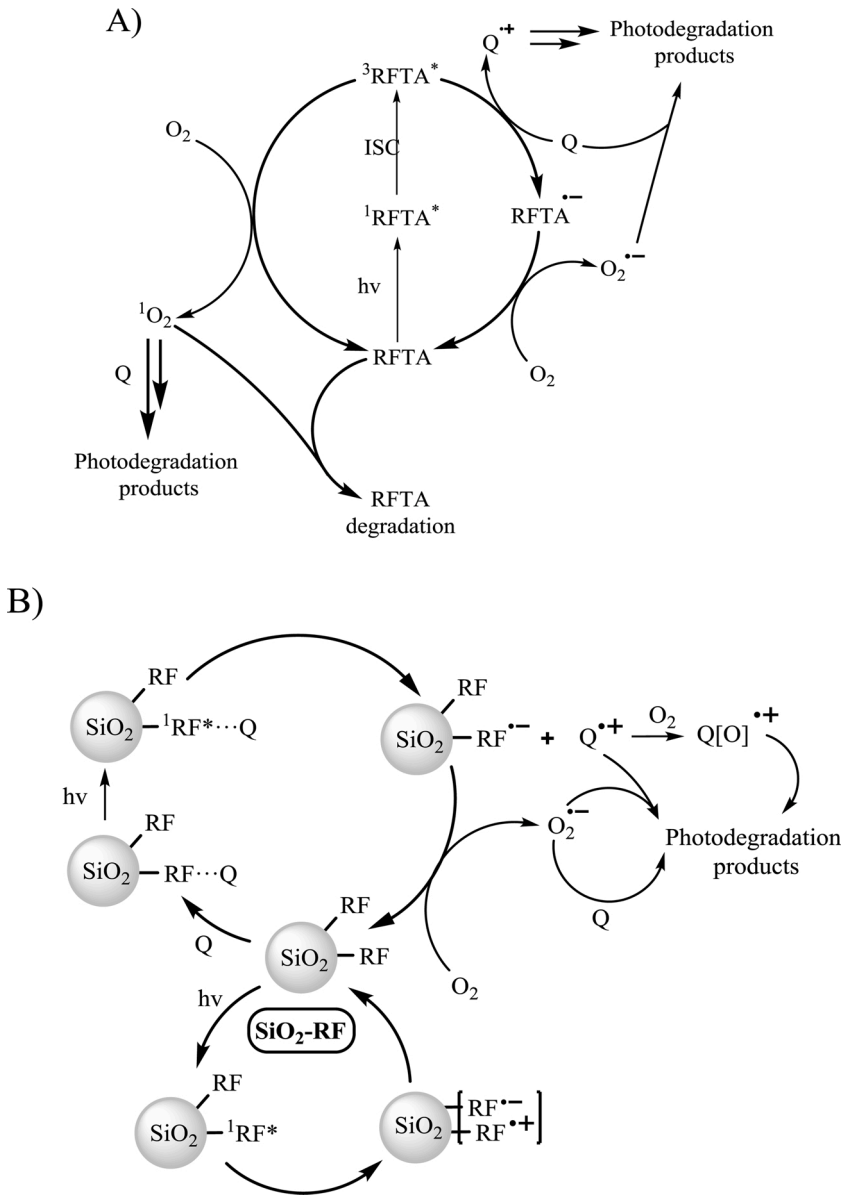

Scheme 3. Postulated mechanism to explain the photodegradation of the selected phenolic pollutants (Q) by RFTA (A) and **SiO$_2$-RF** (B) under visible light irradiation.

for these radicals than for RFTA$^{\bullet-}$ and Q$^{\bullet+}$. This is not surprising because of the short distance between the adsorbed Q and RF on the **SiO$_2$-RF**.

Concerning recyclability, the oxidative degradation of RFTA occurring mainly in 1−2 h, would occur mainly *via* $^1O_2$ reaction. In fact, the $^1O_2$ generation increases at the Q concentration decreases, because O_2 and Q are competing for ^{3}RFTA*; therefore degradation of RFTA is accelerated upon irradiation time. The absence of all these processes in the photodegradation performed using **SiO$_2$-RF** explains the reuse capability of the new synthesized heterogeneous photocatalyst.

Scheme 3 summarizes the main photocatalytic processes involved in the pollutants degradation (Q) photocatalyzed by **SiO$_2$-RF**, as well as those produced by homogeneous RFTA. Consequently, electron transfer from the pollutants to **SiO$_2$-^{1}RF*** is the key process in the heterogeneous photodegradation. In this context, the participation of molecular oxygen was evidenced performing the study under anaerobic conditions. In fact, the absence of oxygen produces longer half-lives for all pollutants (Fig. 9). Although the participation of $^1O_2$ was discarded from the photophysical experiments, direct reaction between O_2 and the radical cations of pollutants (Q$^{\bullet+}$), and formation of the reactive superoxide radical anion ($O_2^{\bullet-}$) from molecular oxygen reduction by **SiO$_2$-RF**$^{-}$ would be involved in the photodegradation of Q. Interestingly, in the absence of adsorbed pollutants, the **SiO$_2$-^{3}RF*** is not formed due to a deactivation pathway mediated by electron transfer between a RF moiety in its singlet excited state and a close ground state RF (see the bottom cycle of Scheme 3B).

5. Conclusions

SiO$_2$-RF, a novel, robust and recyclable organic heterogeneous photocatalyst based on RF is presented. Silica particles have offered a suitable surface to allow covalent derivatization of RF, converting the already known homogeneous photocatalyst into a new and more reliable heterogeneous one. Because of a careful design, formation of the triplet excited state and the subsequent singlet oxygen is prevented, which results in enhanced photostability. Adsorption of the pollutants on the surface of **SiO$_2$-RF** allows electron transfer from the pollutants to the short-lived first singlet excited state of RF, which is consistent with the observed photocatalytic behavior. Photophysical experiments have

provided clear evidence of a new operating photocatalytic mechanism for riboflavin chromophore in **SiO_2-RF**. Moreover, it has been demonstrated that the behavior of anchored RF cannot be predicted from the photophysical and photochemical behavior of RFTA in homogeneous media. Finally, it is noteworthy that these findings open opportunities to design new robust heterogeneous organic photocatalysts for abatement of pollutants in aqueous media.

CRediT authorship contribution statement

Oscar Cabezuelo: Investigation, Methodology, Formal analysis, Writing - original draft. **Rebeca Martinez-Haya:** Investigation, Methodology, Writing - review & editing, Supervision. **Noelia Montes:** Investigation, Methodology. **Francisco Bosca:** Conceptualization, Supervision, Writing - review & editing, Funding acquisition. **M. Luisa Marin:** Conceptualization, Supervision, Writing - review & editing, Funding acquisition.

Declaration of Competing Interest

The authors report no declarations of interest.

Acknowledgements

The authors would like to acknowledge H2020/Marie Skłodowska-Curie Actions under the AQUAlity project (Reference: 765860), Consellería d'Educació, Investigació, Cultura i Esport (PROMETEO/2017/075), the Spanish Ministry of Science, Innovation and Universities (PID2019-110441RB-C33 and SEV-2016-0683). O. Cabezuelo is indebted to the Universitat Politècnica de València for the Predoctoral FPI fellowship (FPI-UPV/Subprograma 1). R. M.-H. acknowledges Fondo Social Europeo (FSE) 2014-2020 Generalitat Valenciana (APOSTD-2019/124).

Appendix A. Supplementary data

Supplementary material related to this article can be found, in the online version, at doi:https://doi.org/10.1016/j.apcatb.2021.120497.

References

[1] W. Gernjak, T. Krutzler, A. Glaser, S. Malato, J. Caceres, R. Bauer, A.R. Fernández-Alba, Photo-fenton treatment of water containing natural phenolic pollutants, Chemosphere 50 (2003) 71–78, https://doi.org/10.1016/S0045-6535(02)00403-4.

[2] S. Chiron, A. Fernandez-Alba, A. Rodriguez, E. Garcia-Calvo, Pesticide chemical oxidation: state-of-the-art, Water Res. 34 (2000) 366–377, https://doi.org/10.1016/S0043-1354(99)00173-6.

[3] M.M. Häggblom, Ingeborg D. Bossert, Halogenated organic compounds – a global perspective, in: M.M. Häggblom, I. Bossert (Eds.), Dehalogenation Microb. Process. Environ. Appl., Mass, Kluwer Academic Publishers, Boston, 2003, pp. 3–29.

[4] U.G. Ahlborg, T.M. Thunberg, H.C. Spencer, Chlorinated phenols: occurrence, toxicity, metabolism, and environmental impact, CRC Crit. Rev. Toxicol. 7 (1980) 1–35, https://doi.org/10.3109/10408448009017934.

[5] A.O. Olaniran, E.O. Igbinosa, Chlorophenols and other related derivatives of environmental concern: properties, distribution and microbial degradation processes, Chemosphere 83 (2011) 1297–1306, https://doi.org/10.1016/j.chemosphere.2011.04.009.

[6] ATSRD, Comprehensive environmental response. Compensation and Liability Act (CERCLA): Priority List of Hazardous Substances, 2007.

[7] OMS, The WHO Recommended Clasification of Pesticides by Hazard, 2019.

[8] R. Andreozzi, V. Caprio, A. Insola, R. Marotta, Advanced oxidation processes (AOP) for water purification and recovery, Catal. Today 53 (1999) 51–59, https://doi.org/10.1016/S0920-5861(99)00102-9.

[9] O. Legrini, E. Oliveros, A.M. Braun, Photochemical processes for water treatment, Chem. Rev. 93 (1993) 671–698, https://doi.org/10.1021/cr00018a003.

[10] M.L. Marin, L. Santos-Juanes, A. Arques, A.M. Amat, M.A. Miranda, Organic photocatalysts for the oxidation of pollutants and model compounds, Chem. Rev. 112 (2012) 1710–1750, https://doi.org/10.1021/cr2000543.

[11] S. Malato, J. Blanco, A. Campos, J. Cáceres, C. Guillard, J.M. Herrmann, A. R. Fernández-Alba, Effect of operating parameters on the testing of new industrial titania catalysts at solar pilot plant scale, Appl. Catal. B Environ. 42 (2003) 349–357, https://doi.org/10.1016/S0926-3373(02)00270-9.

[12] W. Chen, J.J. Chen, R. Lu, C. Qian, W.W. Li, H.Q. Yu, Redox reaction characteristics of riboflavin: a fluorescence spectroelectrochemical analysis and density functional theory calculation, Bioelectrochemistry 98 (2014) 103–108, https://doi.org/10.1016/j.bioelechem.2014.03.010.

[13] J.P. Escalada, A. Pajares, J. Gianotti, A. Biasutti, S. Criado, P. Molina, W. Massad, F. Amat-Guerri, N.A. García, Photosensitized degradation in water of the phenolic pesticides bromoxynil and dichlorophen in the presence of riboflavin, as a model of their natural photodecomposition in the environment, J. Hazard. Mater. 186 (2011) 466–472, https://doi.org/10.1016/j.jhazmat.2010.11.026.

[14] W. Massad, S. Criado, S. Bertolotti, A. Pajares, J. Gianotti, J.P. Escalada, F. Amat-Guerri, N.A. García, Photodegradation of the herbicide Norflurazon sensitised by Riboflavin. A kinetic and mechanistic study, Chemosphere 57 (2004) 455–461, https://doi.org/10.1016/j.chemosphere.2004.06.021.

[15] E. Haggi, S. Bertolotti, N.A. García, Modelling the environmental degradation of water contaminants. Kinetics and mechanism of the riboflavin-sensitised-photooxidation of phenolic compounds, Chemosphere 55 (2004) 1501–1507, https://doi.org/10.1016/j.chemosphere.2004.01.016.

[16] S. Criado, A. Pajares, J. Gianotti, G. Stettler, J.P. Escalada, S. Bertolotti, F. Amat-Guerri, N.A. García, Kinetic study of the riboflavin-sensitised photooxygenation of two hydroxyquinolines of biological interest, J. Photochem. Photobiol. B, Biol. 71 (2003) 19–25, https://doi.org/10.1016/S1011-1344(03)00093-9.

[17] J.S. Miller, Rose bengal-sensitized photooxidation of 2-chlorophenol in water using solar simulated light, Water Res. 39 (2005) 412–422, https://doi.org/10.1016/j.watres.2004.09.019.

[18] D. Gryglik, M. Lach, J.S. Miller, The aqueous photosensitized degradation of butylparaben, Photochem. Photobiol. Sci. 8 (2009) 549–555, https://doi.org/10.1039/b817846a.

[19] L. Carlos, D.O. Mártire, M.C. Gonzalez, J. Gomis, A. Bernabeu, A.M. Amat, A. Arques, Photochemical fate of a mixture of emerging pollutants in the presence of humic substances, Water Res. 46 (2012) 4732–4740, https://doi.org/10.1016/j.watres.2012.06.022.

[20] P.G. Tratnyek, J. Holgné, Oxidation of substituted phenols in the environment: a QSAR analysis of rate constants for reaction with singlet oxygen, Environ. Sci. Technol. 25 (1991) 1596–1604, https://doi.org/10.1021/es00021a011.

[21] M. Pera-Titus, V. García-Molina, M.A. Baños, J. Giménez, S. Esplugas, Degradation of chlorophenols by means of advanced oxidation processes: a general review, Appl. Catal. B Environ. 47 (2004) 219–256, https://doi.org/10.1016/j.apcatb.2003.09.010.

[22] F. Cermola, M. Dellagreca, M.R. Iesce, S. Montella, A. Pollio, F. Temussi, A mild photochemical approach to the degradation of phenols from olive oil mill wastewater, Chemosphere 55 (2004) 1035–1041, https://doi.org/10.1016/j.chemosphere.2003.12.016.

[23] N.A. García, New trends in photobiology. Singlet-molecular-oxygen-mediated photodegradation of aquatic phenolic pollutants. A kinetic and mechanistic overview, J. Photochem. Photobiol. B, Biol. 22 (1994) 185–196, https://doi.org/10.1016/1011-1344(93)06932-S.

[24] G. Porcal, S.G. Bertolotti, C.M. Previtali, M.V. Encinas, Electron transfer quenching of singlet and triplet excited states of flavins and lumichrome by aromatic and aliphatic electron donors, Phys. Chem. Chem. Phys. 5 (2003) 4123–4128, https://doi.org/10.1039/b306945a.

[25] C. Lu, W. Lin, W. Wang, Z. Han, S. Yao, N. Lin, Riboflavin (VB2) photosensitized oxidation of 2'-deoxyguanosine-5'-monophosphate (dGMP) in aqueous solution: a transient intermediates study, Phys. Chem. Chem. Phys. 2 (2000) 329–334, https://doi.org/10.1039/A908492D.

[26] S.L.J. Tan, R.D. Webster, Electrochemically induced chemically reversible proton-coupled electron transfer reactions of riboflavin (Vitamin B 2), J. Am. Chem. Soc. 134 (2012) 5954–5964, https://doi.org/10.1021/ja300191u.

[27] A. Masek, E. Chrzescijanska, M. Zaborski, M. MacIejewska, Characterisation of the antioxidant acitivity of riboflavin in an elastomeric composite, Comptes Rendus Chim. 15 (2012) 524–529, https://doi.org/10.1016/j.crci.2012.01.012.

[28] P.F. Heelis, The photophysical and photochemical properties of flavins (isoalloxazines), Chem. Soc. Rev. 11 (1982) 15–39, https://doi.org/10.1039/CS9821100015.

[29] M. Czaplicka, Photo-degradation of chlorophenols in the aqueous solution, J. Hazard. Mater. 134 (2006) 45–59, https://doi.org/10.1016/j.jhazmat.2005.10.039.

[30] I. Gutiérrez, S. Criado, S. Bertolotti, N.A. García, Dark and photoinduced interactions between Trolox, a polar-solvent-soluble model for vitamin E, and riboflavin, J. Photochem. Photobiol. B, Biol. 62 (2001) 133–139, https://doi.org/10.1016/S1011-1344(01)00170-1.

[31] R.A. Larson, D.D. Ellis, H. -L Ju, K.A. Marley, Flavin-sensitized photodecomposition of anilines and phenols, Environ. Toxicol. Chem. 8 (1989) 1165–1170, https://doi.org/10.1002/etc.5620081209.

[32] E.C. Smith, D.E. Metzler, The photochemical degradation of Riboflavin, J. Am. Chem. Soc. 85 (1963) 3285–3288, https://doi.org/10.1021/ja00903a051.

[33] S. Miskoski, N.A. Garcia, Effect of chlorophenolic pesticides on the photochemistry of riboflavin, Toxicol. Environ. Chem. 25 (1989) 33–43, https://doi.org/10.1080/02772248909357503.

[34] W.M. Moore, J.T. Spence, F.A. Raymond, S.D. Colson, The photochemistry of riboflavin. I. The hydrogen transfer process in the anaerobic photobleaching of flavins, J. Am. Chem. Soc. 85 (1963) 3367–3372, https://doi.org/10.1021/ja00904a013.

[35] N.C. Angeluzzi, M. Muñoz, D.T. Marquez, M.S. Baptista, A.M. Edwards, E. I. Alarcon, J.C. Scaiano, Silica nanoreactors from silylated riboflavin for efficient singlet oxygen delivery, J. Mater. Chem. B 2 (2014) 4221–4225, https://doi.org/10.1039/c4tb00170b.

[36] D. Tarn, C.E. Ashley, M. Xue, E.C. Carnes, J.I. Zink, C.J. Brinker, Mesoporous silica nanoparticle nanocarriers: biofunctionality and biocompatibility, Acc. Chem. Res. 46 (2013) 792–801, https://doi.org/10.1021/ar3000986.
[37] A.I. Carrillo, A. Elhage, M.L. Marin, A.E. Lanterna, Perylene-Grafted Silicas, Mechanistic study and applications in heterogeneous photoredox catalysis, Chem. - A Eur. J. 25 (2019) 14928–14934, https://doi.org/10.1002/chem.201903539.
[38] H. Grajek, I. Gryczynski, P. Bojarski, Z. Gryczynski, S. Bharill, L. Kułak, Flavin mononucleotide fluorescence intensity decay in concentrated aqueous solutions, Chem. Phys. Lett. 439 (2007) 151–156, https://doi.org/10.1016/j.cplett.2007.03.042.
[39] W. Stöber, A. Fink, Controlled growth of monodisperse silica spheres in the micron size range, Journal Colloid Interface Sci. 26 (1968) 62–69, https://doi.org/10.1016/0021-9797(68)90272-5.
[40] D.U. McCormick, Flavin derivatives viw urornination of the 8-Methyl substituent, J. Heterocycl. Chem. 7 (1970) 447–450, https://doi.org/10.1002/jhet.5570070240C.
[41] A.V. Silva, A. López-Sánchez, H.C. Junqueira, L. Rivas, M.S. Baptista, G. Orellana, Riboflavin derivatives for enhanced photodynamic activity against Leishmania parasites, Tetrahedron 71 (2015) 457–462, https://doi.org/10.1016/j.tet.2014.11.072.
[42] L.K. Fraiji, D.M. Hayes, T.C. Werner, Static and dynamic fluorescence quenching experiments for the physical chemistry laboratory, J. Chem. Educ. 69 (1992) 424–428, https://doi.org/10.1021/ed069p424.
[43] B. König, M. Pelka, H. Zieg, T. Ritter, H. Bouas-Laurent, R. Bonneau, J. P. Desvergne, Photoinduced electron transfer in a phenothiazine-riboflavin dyad assembled by zinc-imide coordination in water, J. Am. Chem. Soc. 121 (1999) 1681–1687, https://doi.org/10.1021/ja9836693.
[44] A. Penzkofer, Photoluminescence behavior of riboflavin and lumiflavin in liquid solutions and solid films, Chem. Phys. 400 (2012) 142–153, https://doi.org/10.1016/j.chemphys.2012.03.017.
[45] A.S. Pavitt, E.J. Bylaska, P.G. Tratnyek, Oxidation potentials of phenols and anilines: correlation analysis of electrochemical and theoretical values, Environ. Sci. Process. Impacts 19 (2017) 339–349, https://doi.org/10.1039/c6em00694a.
[46] S.L. Murov, I. Carmichael, G.L. Hug, Handbook of Photochemistry, 2nd ed., 2009, https://doi.org/10.1201/9781420015195. New York.
[47] S.G. Bertolotti, C.M. Previtali, A.M. Rufs, M.V. Encinas, Riboflavin/triethanolamine as photoinitiator system of vinyl polymerization. A mechanistic study by laser flash photolysis, Macromolecules 32 (1999) 2920–2924, https://doi.org/10.1021/ma981246f.
[48] A. Wolnicka-Glubisz, A. Pawlak, M. Insinska-Rak, A. Zadlo, Analysis of photoreactivity and phototoxicity of riboflavin's analogue 3MeTARF, J. Photochem. Photobiol. B, Biol. 205 (2020) 111820, https://doi.org/10.1016/j.jphotobiol.2020.111820.
[49] L. Codognoto, S.A.S. Machado, L.A. Avaca, Selective oxidation of pentachlorophenol on diamond electrodes, J. Appl. Electrochem. 33 (2003) 951–957, https://doi.org/10.1023/A:1025820029412.